










Magnetic and structural properties of the intermetallic $\text{Ce}_{(1-x)}\text{La}_x\text{CrGe}_3$ series of compoundsB. Bosch-Santos ^{1,2,*}, G. A. Cabrera-Pasca ³, E. L. Correa ^{4,2}, B. S. Correa ², T. N. S. Sales ²,
K.-W. Moon ⁴, C. L. Dennis,⁴ Q. Huang,¹ J. B. Leao ¹, J. W. Lynn ¹ and A. W. Carbonari ²¹NIST Center for Neutron Research, National Institute of Standards and Technology, Gaithersburg, Maryland 20899, USA²Instituto de Pesquisas Energéticas e Nucleares IPEN, São Paulo, São Paulo, SP, 05508-000, Brazil³Faculdade de Ciências Exatas e Tecnologia, Universidade Federal do Pará, Abaetetuba, PA, 68440-000, Brazil⁴Material Measurement Laboratory, National Institute of Standards and Technology - NIST, Gaithersburg, Maryland 20899, USA

(Received 31 August 2021; accepted 3 November 2021; published 22 November 2021)

The $\text{Ce}_{(1-x)}\text{La}_x\text{CrGe}_3$ ($x = 0, 0.19, 0.43, 0.58,$ and 1) intermetallic compound system has been investigated by magnetization measurements and neutron scattering techniques to determine the effect of La doping on the magnetic ordering and exchange interaction between Cr ions. The structural and magnetic characterization in this series was first verified by x-ray diffraction and bulk magnetization measurements. The samples exhibit the known hexagonal perovskite structure ($P6_3/mmc$ space group) and have a single magnetic phase according to magnetization measurements. In this paper, the ferromagnetic ordering temperature for Cr evolves smoothly from a range of 68 K to 77 K for CeCrGe_3 to a range of 91 K to 96 K for LaCrGe_3 as La replaces Ce. Magnetization results indicate the formation of domain walls below the transition temperature for all $\text{Ce}_{(1-x)}\text{La}_x\text{CrGe}_3$ systems investigated. Neutron results indicate ordered magnetic Cr moments aligned along the c axis for the $x = 1$ LaCrGe_3 system, as well as for $x = 0.19, 0.43,$ and $0.58,$ which contrasts with the $x = 0$ CeCrGe_3 where the moments order in the ab plane.

DOI: [10.1103/PhysRevMaterials.5.114406](https://doi.org/10.1103/PhysRevMaterials.5.114406)

I. INTRODUCTION

Compounds with rare-earth (R) and transition metal (TM) elements are interesting magnetic systems due to the possibility of magnetic coupling between the R and TM atoms. Around 15 years ago, intermetallic systems containing R and TM (RTMGe_3 with $\text{TM} = \text{Ti}, \text{Cr}$) were discovered [1,2] that had an unusual feature: they crystalize in the perovskite-type structure (space group $P6_3/mmc$) and can exhibit a wide variety of interesting properties including dense Kondo lattice behavior, long-range magnetic order, quantum criticality, heavy fermion physics, and superconductivity.

For compounds of this family where the magnetic behavior originates solely from R ions, they typically order at low temperatures where Kondo lattice, heavy fermion behavior, and/or superconductivity can emerge, and they are called heavy-fermion compounds. For example, the magnetic ordering of the Ce moment occurs at 5.5 K in CeNiGe_3 , 14.5 K in CeRhGe_3 , and 14 K in CeTiGe_3 . All these compounds are heavy fermions [3,4]. Furthermore, the TM ions in these compounds have no magnetic moment so the magnetic behavior originates from the R atoms [5]. By contrast, in RCrGe_3 the Cr atoms exhibit magnetic moments which order ferromagnetically at much higher temperatures, as indicated by the end member LaCrGe_3 of particular interest here where R magnetic moments are absent [2]. One of the interesting aspects of this system is that the ferromagnetism can be suppressed toward a purported quantum critical point (QCP) by doping

[6], pressure, or applied magnetic field [7,8]. However, with the introduction of magnetic R 's, the emergence of magnetic interactions between the Cr atoms and the $4f$ - R moments presents an interesting situation for this strongly correlated electron system. In these compounds, the ground state is ruled to a large extent by two competitive interactions: Ruderman-Kittel-Kasuya-Yosida indirect exchange, and Kondo exchange [2,9]. This RCrGe_3 system then may have the potential to evade the QCP.

Specifically, LaCrGe_3 and CeCrGe_3 are two interesting end members of this family due to the fact that Ce has one $4f$ electron and La has no $4f$ electron. Furthermore, previous reports have shown that LaCrGe_3 has a fragile magnetism and CeCrGe_3 is a moderate heavy-fermion system [10,11]. A neutron diffraction investigation of the fragile ferromagnet LaCrGe_3 shows that the Cr moments are aligned along the c axis below the ordering temperature of 78 K, but have a spin-canted structure below 3 K. At 1.7 K, the spins form an angle of 32° with respect to the c axis [12]. On the other hand, the alignment of Cr moments in the moderate heavy-fermion CeCrGe_3 is still under discussion; previous work has shown the possibility of analyzing the same neutron diffraction data using two very different assumptions: Cr spins parallel to the ab plane or parallel to the c -axis direction. Results from both models are quite different and, therefore, further investigation is necessary. The presence of Ce magnetic moments in CeCrGe_3 can induce both the Ce and Cr moments to be aligned in the ab plane in the ferromagnetic phase, as shown by neutron diffraction [9]. Controversially, a study using muon spin relaxation has not shown ordering of the Ce moments [5]. Finally, an interesting characteristic

*brianna@alumni.usp.br

of CeCrGe_3 is that it has been shown to present the Kondo effect with heavy-fermion behavior, where Ce atoms have an integral +3 valence state [10].

Previous work has presented several values for the magnetic transition temperature. The ferromagnetic transition temperature in LaCrGe_3 is reported to vary from 78 K to 88 K [2,8,10,12], whereas for CeCrGe_3 , this temperature can vary from 66 K to 73 K [2,10]. Furthermore, there are claims of the existence of a tricritical point near 40 K for LaCrGe_3 when external pressure is applied [8].

Despite the interest in this family of compounds, the understanding of these materials remains elusive. CeCrGe_3 and LaCrGe_3 have been reported to present different collinear alignments of the Cr spins: In LaCrGe_3 , the alignment is along the c axis whereas in CeCrGe_3 it is an unresolved issue [9,12]. These issues, including the Cr spin alignment in CeCrGe_3 , the possible difference in its alignment in CeCrGe_3 and LaCrGe_3 , and the possible ordering of the Ce moments, have motivated us to investigate the La doping in the CeCrGe_3 to ascertain the influence of the $4f$ electron in the magnetic behavior of doped compounds. In addition, the fragile magnetism of LaCrGe_3 appears to be due to the Cr d orbital possessing a peak just below the Fermi level. Modest changes in pressure can then cause substantial changes in the magnetic characteristics [11]. This pressure can be a chemical pressure or physical pressure; in this paper, the La substitution by Ce will cause a decrease in the crystal cell volume. Another interesting aspect that was not well studied, and reported by Bie *et al.*, is the magnetic domain formation in the family of compounds RCrGe_3 ($R = \text{La-Nd, Sm}$) [2]. Afterward, Lemoine *et al.* investigated the magnetic domain formation and domain-wall movement in NdCrGe_3 [13]. These are important properties to be investigated due to their influence on the magnetic transition temperature, magnetic moment, and spin alignment [13–16].

In this paper, we have combined neutron-scattering techniques and magnetization measurements to investigate the magnetic properties of the series $\text{Ce}_{(1-x)}\text{La}_x\text{CrGe}_3$ ($x = 0, 0.19, 0.43, 0.58, \text{ and } 1$). Results from the magnetization measurements revealed the formation of domain walls for all compounds in this series. Moreover, NPD demonstrated that the Cr moments align along the c axis for $x = 0.19, 0.43, 0.58, \text{ and } 1$ and align in the ab plane for $x = 0$. Here we discuss the contrast in the alignment direction of the Cr moments, the large difference in the values of effective magnetic moment and ordered magnetic moment, as well as the divergence between the temperature transition values determined using magnetization measurements and neutron diffraction.

II. EXPERIMENTAL DETAILS

Intermetallic $\text{Ce}_{(1-x)}\text{La}_x\text{CrGe}_3$ ($x = 0, 0.19, 0.43, 0.58, 1$) compounds were prepared by arc melting in an argon atmosphere. Starting elements of La and Ce pieces with 99.9% purity and Cr and Ge pieces with 99.999% purity were added in the stoichiometric ratio. After melting, the resulting ingot of each sample was sealed in an evacuated quartz tube ($\sim 10^{-2}$ Pa), which was then annealed at 900 °C for two weeks. After annealing, the structural quality of the samples was verified by x-ray diffraction (XRD) (Rigaku Ultima III) with $\text{Cu-K}\alpha$ radiation. The CeCrGe_3 , LaCrGe_3 ,

and $\text{Ce}_{0.58}\text{La}_{0.43}\text{CrGe}_3$ samples were single phase, corresponding to the expected hexagonal perovskite-type structure with space group $P6_3/mmc$ as previously reported [2]. $\text{Ce}_{0.42}\text{La}_{0.58}\text{CrGe}_3$ and $\text{Ce}_{0.81}\text{La}_{0.19}\text{CrGe}_3$ samples showed an additional small impurity phase ($< 1\%$ and around 6%, respectively). The impurity phase was identified as $\text{La}(\text{Ce})\text{Ge}_2$ crystallized in the tetragonal structure with space group $I4_1/amd$. This phase forms at 1500 °C and is a common impurity found in these types of compounds when prepared by arc melting [17]. All intermetallic samples were prepared in the Hyperfine Interactions Laboratory at the Nuclear and Energy Research Institute, except the $\text{Ce}_{0.8}\text{La}_{0.2}\text{CrGe}_3$ sample that was prepared at National Institute of Standard and Technology (NIST).

To investigate the macroscopic magnetic properties, samples were magnetically characterized using a Superconducting Quantum Interference Device Vibrating-Sample Magnetometer (SQUID-VSM, Quantum Design). The characterization was performed after cooling the sample in zero field by measuring the DC magnetic moment (M) at $\mu_0 H = 0.01$ T while warming followed by cooling. The first curve, after the zero field cool, is referred to as the ZFC data. The second curve, measured while cooling under an applied field, is referred to as the FC data. M versus T was then converted to $\chi_{\text{DC}}(T)$, where $\chi_{\text{DC}} = M/H$. In addition, the AC susceptibility [both real (χ') and imaginary (χ'') components] as a function of temperature for different frequencies $f = 1$ Hz, 10 Hz, and 100 Hz and AC field of 10^{-4} T, was measured. These were performed to cross check the features observed in the DC magnetization measurements and to discard any other possible magnetic phase occurring in the system due to the La doping.

To study the magnetic structure and better understand the magnetic behavior in this series, neutron diffraction data were obtained at the NIST Center for Neutron Research (NCNR). For both neutron powder diffraction (NPD) measurements using high resolution or coarse resolution/high intensity, the mass of the polycrystalline powder samples used in the measurements was around 1.3 g for $\text{Ce}_{(1-x)}\text{La}_x\text{CrGe}_3$ ($x = 0, 0.43, 0.58, 1$) and ~ 4 g for the $\text{Ce}_{0.81}\text{La}_{0.19}\text{CrGe}_3$. Each sample was sealed in a vanadium container under helium atmosphere in a glove box. NPD data were collected using the BT-1 32-detector high-resolution neutron powder diffractometer at NCNR [18] over the range $2\theta = 3^\circ$ to $2\theta = 168^\circ$ with a step size of 0.050° . For all samples, measurements were taken at 5 K, 295 K, and at a temperature slightly above the magnetic transition temperature determined by magnetization measurements. Temperature-dependent data sets were obtained using a closed cycle refrigeration system. A Cu (311) monochromator (wavelength $\lambda = 1.5402$ (2) Å) with a take-off angle of 90° and 60 min of arc in-pile collimation was used to collect room temperature data. A Ge (311) monochromator [$\lambda = 2.0787$ (2) Å] and in-pile collimation of 60 min of arc was used for the low-temperature measurements due to its higher resolution at low angles. Rietveld refinement was used to solve the nuclear and magnetic structure for all patterns and it was performed using Generalized Structure Analysis System (GSAS) software [19]. The temperature dependence of the magnetic Bragg peaks and the order parameters were obtained from measurements at the BT-7 triple-axis spectrometer [20] at NCNR. Measurements were carried out using a pyrolytic

TABLE I. Results obtained by fitting the modified Curie-Weiss law to χ^{-1} for CeCrGe₃, Ce_{0.81}La_{0.19}CrGe₃ ($x = 0.19$), Ce_{0.58}La_{0.43}CrGe₃ ($x = 0.43$), Ce_{0.42}La_{0.58}CrGe₃ ($x = 0.58$), and LaCrGe₃: Curie temperature ($T_C^{(DC)}$ and $T_C^{(AC)}$), Curie-Weiss temperature (θ_{CW}), and effective magnetic moment (μ_{eff}). Values of $\mu_{eff}(y)$ are the estimate μ_{eff} values considering Ce³⁺ and Cr³⁺ ions and the Ce percentage in each sample. T_C and μ_{eff} from literature are also displayed. The numbers between parentheses are shown the error bars and represent 1 σ .

Sample	$T_C^{(DC)}$ (K)	$T_C^{(AC)}$ (K)	θ_{CW} (K)	C (K.A/T.m)	μ_{eff} (μ_B /Cr)	$\mu_{eff}(y)$ (μ_B)	lit. T_C (K)	lit. μ_{eff} (μ_B /Cr)
CeCrGe ₃	68.0(1)	68.6(4)	74.4(2)	32.1(3)	3.23(2)	4.57	73 ^a , 70 ^b	3.18 ^a , 3.36 ^b
$x = 0.19$	73.8(1)	73.8(3)	78.8(3)	43.6(6)	3.77(3)	4.43	—	—
$x = 0.43$	77.8(1)	78.2(2)	84.1(5)	48.8(3)	4.00(5)	4.26	—	—
$x = 0.58$	81.8(1)	83.8(2)	90.5(2)	26.7(4)	2.94(2)	4.14	—	—
LaCrGe ₃	91.4(1)	96.8(8)	98.6(2)	18.5(2)	2.46(2)	3.8	86 ^c , 88 ^a	2.38 ^c , 2.66 ^a

^aReported by Das *et al.* [10].

^bReported by Das *et al.* [5].

^cReported by Taoufour *et al.* [7].

graphite [PG (002)] monochromator with wavelength 2.359 Å. The data were taken using 80' to 80' open collimation before the sample, and an 80' radial collimator in front of the position sensitive detector, and scattering angles of $2\theta = 13^\circ$ to $2\theta = 103^\circ$. Samples were measured in powder form inside a vanadium can under low pressure He gas. Measurements were performed in a closed cycle refrigerator with a range of temperatures from 2 K to 120 K for Ce_(1-x)La_xCrGe₃ ($x = 0.19, 0.43, 0.58, 1$). CeCrGe₃ was first measured in a temperature range of 2 K to 10 K to verify the magnetic transition from the Ce spins, and then from 10 K to 120 K. The magnetic peak scattering was located in the (100) plane for all samples. All BT-7 data were analyzed using Data Analysis and Visualization Environment software [21]. The error bars in Fig. 12 (Sec. IV, Discussion) are the standard deviations of the adjusted parameters from GSAS software. For lattice parameters, the error is 0.001 and for unit cell volume the error is 0.1³, as shown in Table II.

III. EXPERIMENTAL RESULTS

A. Magnetization measurements

Magnetization measurement results are displayed in Fig. 1 for CeCrGe₃ and LaCrGe₃, and Fig. 2 for Ce_{0.81}La_{0.19}CrGe₃ ($x = 0.19$), Ce_{0.58}La_{0.43}CrGe₃ ($x = 0.43$), and Ce_{0.42}La_{0.58}CrGe₃ ($x = 0.58$). For $\chi_{DC}(T)$, all samples show a clear ferromagnetic-paramagnetic transition. The ZFC and FC data demonstrate a clear turn-up after which $\chi_{DC}(T)$

increases rapidly with decreasing temperature [see Figs. 1(a) and 2(a)]. Also, a divergence between ZFC and FC curves below the temperature transition can be seen. This behavior is likely due to magnetic domains, which indicate a strong magnetocrystalline anisotropy, as has been presented by Bie *et al.* in RCrGe₃ ($R = \text{La-Nr, Sm}$) [2] and Lemoine *et al.* in NdCrGe₃ [13]. Additionally, LaCrGe₃ in the ZFC curve [see Fig. 1(a)] presents a little bump around 80 K, suggesting a possible spin reorientation or the coexistence of both antiferromagnetic and ferromagnetic phases.

Above the magnetic transition temperature (in the paramagnetic phase), $\chi_{DC}(T)$ shows characteristic Curie-Weiss behavior for paramagnetic states. In the case of doped samples ($x = 0.19, 0.43, \text{ and } 0.58$), the inverse $\chi_{DC}(T)$ data have shown a nonlinear behavior that present a smooth curvature [see Fig. 2(b)]. Hence, the inverse of modified Curie-Weiss law was used to fit the data, described by $\chi = C/(T - \theta_{CW}) + \chi_0$ and fit in the paramagnetic region. Here C is the Curie constant, θ_{CW} is the Curie-Weiss temperature, and χ_0 is the temperature-independent susceptibility [22]. From the fit of χ^{-1} [see Figs. 1(b) and 2(b)], C and θ_{CW} can be calculated and the results are used to determine the effective magnetic moment given by $\mu_{eff} = (2.828 \times \sqrt{C \times MM})\mu_B$, where MM is the molecular mass of each compound. The ferromagnetic ordering temperature ($T_C^{(DC)}$) values were determined by the minimum of the derivative ($d\chi/dT$) of the ZFC curve [see Figs. 1(c) and 2(c)]. The values obtained from the fits, as well as the $T_C^{(DC)}$ of different quantities of La doping, are shown in

TABLE II. Structural parameters obtained from the neutron Rietveld refinement analysis of measurements taken at 295 K on Ce_(1-x)La_xCrGe₃ ($x = 0, 0.19, 0.43, 0.58, 1$) series: Unit cell parameters (a and c), Ge atom position (x_{Ge} and y_{Ge}), and chi squared (quality of the fit) (χ^2).

	CeCrGe ₃	Ce _{0.81} La _{0.19} CrGe ₃	Ce _{0.58} La _{0.43} CrGe ₃	Ce _{0.42} La _{0.58} CrGe ₃	LaCrGe ₃
a (Å)	6.140(1)	6.153(1)	6.165(1)	6.168(1)	6.176(1)
c (Å)	5.711(1)	5.723(1)	5.735(1)	5.737(1)	5.745(1)
Occ(Ce)	—	0.81(2)	0.58(2)	0.42(1)	—
Occ(La)	—	0.19(2)	0.43(2)	0.58(1)	—
x_{Ge}	0.1928(1)	0.1930(1)	0.1931(1)	0.1931(1)	0.1930(1)
y_{Ge}	0.3856(1)	0.3861(1)	0.3863(1)	0.3862(1)	0.3860(2)
χ^2	0.8889	1.30	0.9609	1.092	0.930

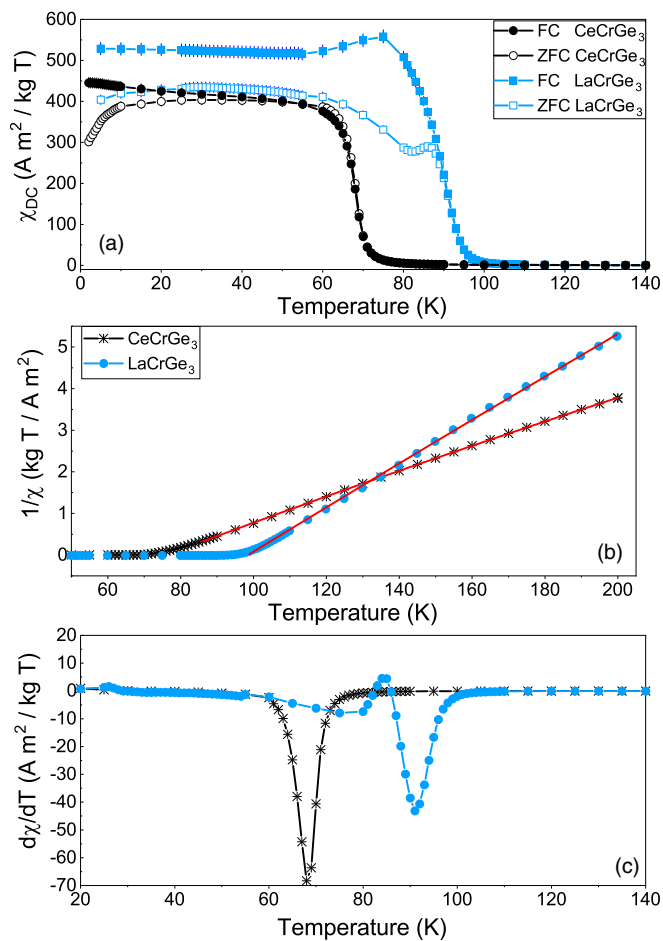


FIG. 1. (a) FC and ZFC χ_{DC} for CeCrGe₃ and LaCrGe₃. (b) Inverse of χ_{DC} as a function of temperature. Solid lines are the modified Curie-Weiss law fit. (c) Derivative of DC susceptibility as a function of temperature. All error bars are shown and represent 1σ . However, the error bars may be smaller than the symbol.

Table I. Note that to obtain the ferromagnetic ordering temperature ($T_C^{(AC)}$) from $\chi_{AC}(T)$ data, we have used the minimum of the derivative ($d\chi_{AC}/dT$) of the real part (χ') curve [see Figs. 3(c) and 4(c)].

As shown in Table I, μ_{eff} displays a peak, with the values for the doped samples being higher than the values for pure samples (CeCrGe₃ and LaCrGe₃). To estimate the value of μ_{eff} in the doped samples, considering the Ce contribution, we used the equation $\mu_{eff}(y) = \sqrt{(\mu_{Ce^{3+}})^2(y) + (\mu_{Cr^{3+}})^2\mu_B}$, where y is the Ce quantity. We are not considering Cr⁴⁺ because, from data of density of states curves, the compound LaCrGe₃ presents the general formulation (La³⁺)(Cr³⁺)(Ge²⁻)₃ [2]. Furthermore, we assume in our samples that Ce is trivalent because Ce⁴⁺ has the 4f⁰ orbital and therefore has no magnetic contribution. Thus, from previous x-ray absorption spectroscopy results, we use the following values: Cr³⁺ (3.8 μ_B) and Ce³⁺ (2.54 μ_B) [10]. The estimated values of μ_{eff} are displayed in Table I.

In Table I, the positive values of Curie-Weiss temperatures for all samples confirm net ferromagnetic interactions in this system. Previous works have reported T_C and μ_{eff} results from magnetization measurements for LaCrGe₃ and CeCrGe₃

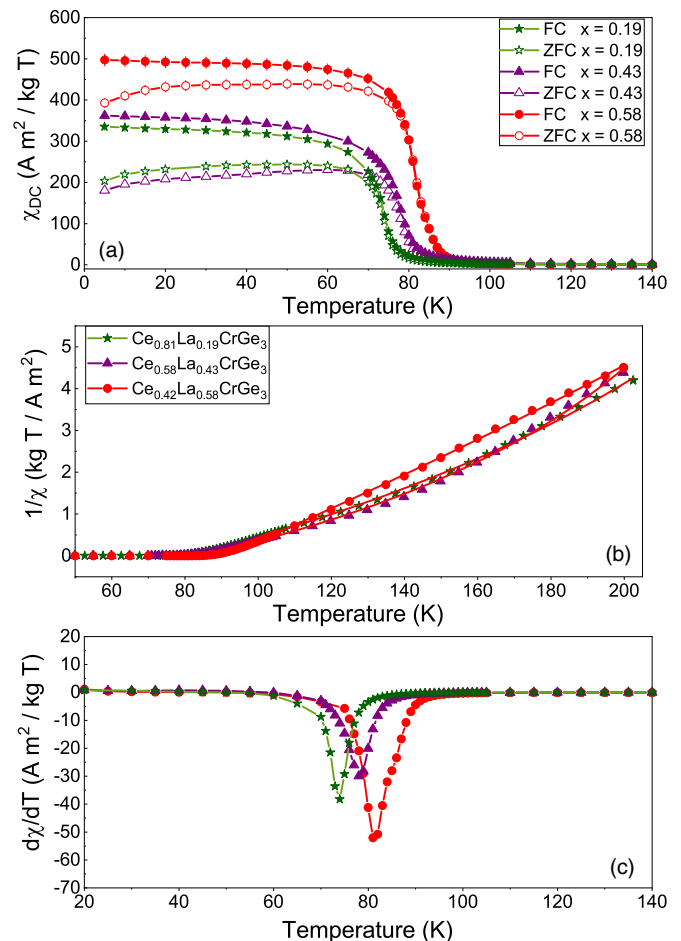


FIG. 2. (a) FC and ZFC χ_{DC} for Ce_(1-x)La_xCrGe₃ ($x = 0.19, 0.43, 0.58$). (b) Inverse of χ_{DC} as a function of temperature. Solid lines are the modified Curie-Weiss law fit. (c) Derivative of DC susceptibility as a function of temperature. All error bars are shown and represent 1σ . However, the error bars may be smaller than the symbol.

[5,7,10]. Values of $T_C^{(DC)}$ and $T_C^{(AC)}$ show a displacement when compared to those reported in the literature, as can be seen in Table I, except $T_C^{(AC)}$ for CeCrGe₃, which is in good agreement with that from Das *et al.* [5]. We do not have enough data to explain this discrepancy. Overall, values of μ_{eff} agree reasonably well with those from literature. Interestingly, the calculated values for μ_{eff} are linear with La doping, but the measured values are not. This does imply that there is another factor involved which has not yet been accounted for. Since the Curie-Weiss fits are in the paramagnetic phase, we can expect contributions from the magnetic moments but these moments will not necessarily couple at low temperature. Therefore, μ_{eff} found using the Curie-Weiss law should not be higher than μ_{eff} for the free ion, as was the case.

$\chi_{AC}(T)$ [both (χ') and (χ'') component] curves are shown in Figs. 3(a) and 3(b) for Ce_(1-x)La_xCrGe₃ ($x = 0, 0.19, 0.43, 0.58$) and Figs. 4(a) and 4(b) for LaCrGe₃. As can be seen, for all samples there is a clear upturn in the χ' component with decreasing temperature, characteristic of the paramagnetic-ferromagnetic transition. Below this transition, the $\chi_{AC}(T)$

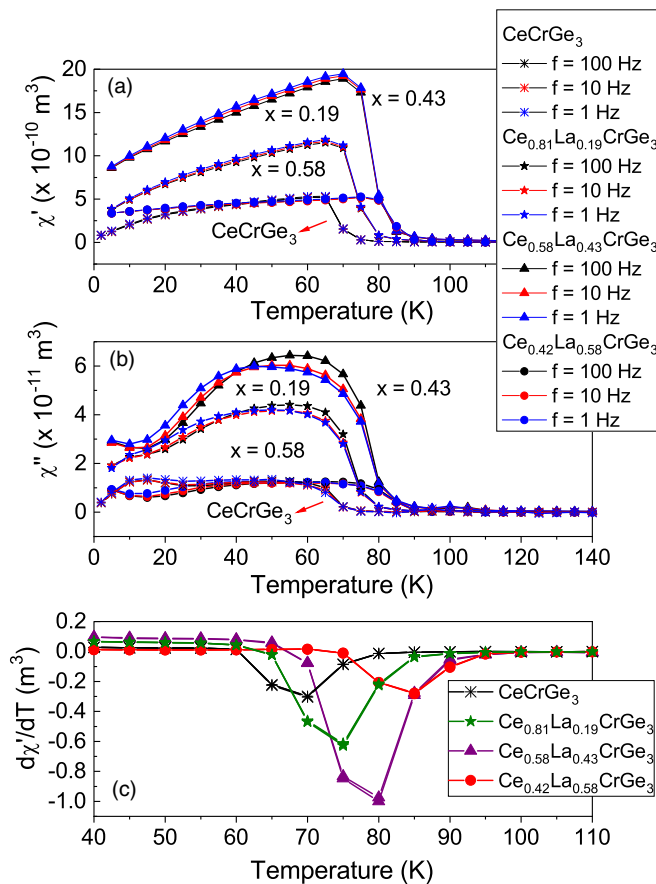


FIG. 3. χ_{AC} for $Ce_{(1-x)}La_xCrGe_3$ ($x = 0, 0.19, 0.43, 0.58$) (a) real component (χ'). (b) Imaginary component (χ'') and (c) derivative of χ_{AC} real component as a function of temperature. All error bars are shown and represent 1σ . However, the error bars may be smaller than the symbol.

[[χ'] and (χ'')] curves for the $CeCrGe_3$ and doped samples ($x = 0.19, 0.43$, and 0.58) display typical ferromagnetic behavior, with a smooth decrease of the magnetic susceptibility below T_C [see Figs. 3(a) and 3(b)]. This decrease in χ' usually occurs due to a reduction in the ability of the material to respond to the low AC magnetic field (here 10^{-14} T) [23]. The decrease in χ'' likely occurs due to the formation of domain walls and magnetic domains within the material that absorb energy when they are pinned while trying to grow/shrink [23]. This is most evident in $x = 0$, $x = 0.19$, and $x = 0.43$ samples.

On the other hand, for $LaCrGe_3$ the behavior of χ' is related to the magnetic domain structure, which appears right below T_C . With the decrease in temperature, it is clear that the material loses its ability to respond to the AC magnetic field. For example, if multiple pinned domains form just below T_C and the excitation field is not large enough to shift the moment, then the AC response can shift to near zero. In χ'' , a similar peak can be seen in the same temperature range, corroborating the formation of magnetic domains, which absorb energy while trying to move them. Also, at lower temperatures (20–30 K), a second larger peak can be seen in both χ' and χ'' , further supporting this explanation. Alternatively, the second

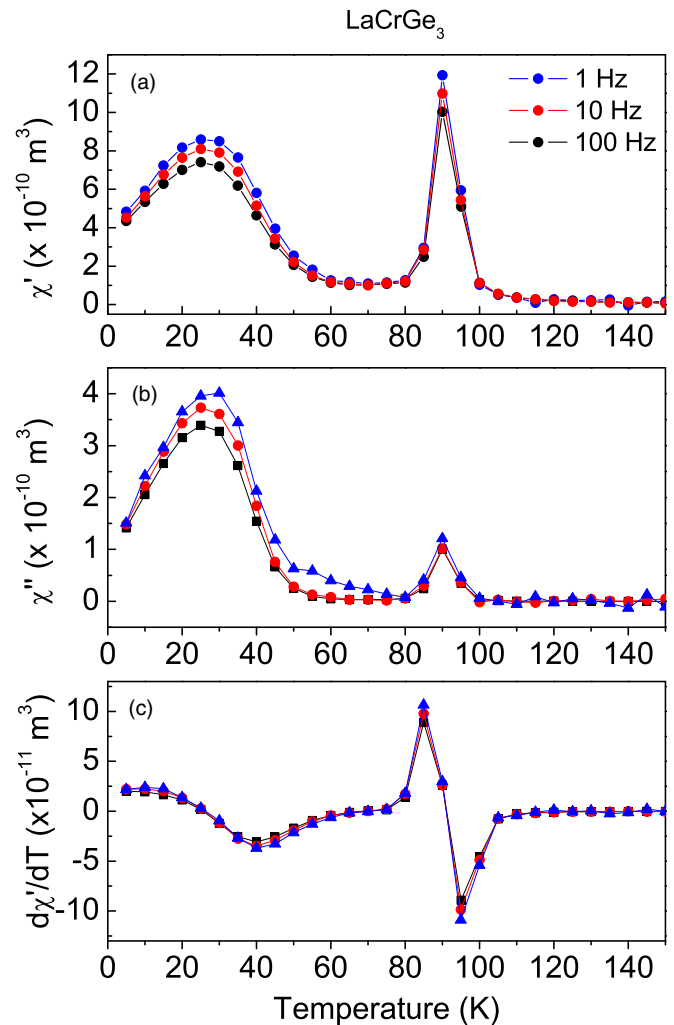


FIG. 4. χ_{AC} for $LaCrGe_3$ (a) real component (χ') (b) imaginary component (χ'') and (c) Derivative of χ_{AC} real component as a function of temperature. All error bars are shown and represent 1σ . However, the error bars may be smaller than the symbol.

peak in χ'' could be related to spin-glass behavior. However, despite the frequency dependence, a change in the peak position as a function of the temperature is not observed [24].

B. Neutron measurements

1. Neutron powder diffraction at BT-1

Similar to what is observed with XRD measurements, $CeCrGe_3$, $LaCrGe_3$, and $Ce_{0.58}La_{0.43}CrGe_3$ exhibit a single phase of the expected hexagonal perovskite-type structure with space group $P6_3/mmc$, without observable impurities. On the other hand, $Ce_{0.42}La_{0.58}CrGe_3$ and $Ce_{0.81}La_{0.19}CrGe_3$ show less than 1% and around 6% of a secondary phase, respectively. In both cases, the secondary phases were identified as the $La(Ce)Ge_2$ tetragonal phase with space group $I4_1/amd$ (see the peaks distinguished by the symbol * and inset in Fig. 6). As explained in related papers [9,12], the appearance of this impurity in these compounds is common due to the high temperature used in the arc melting. Nevertheless, such secondary phases are nonmagnetic and their atomic peak

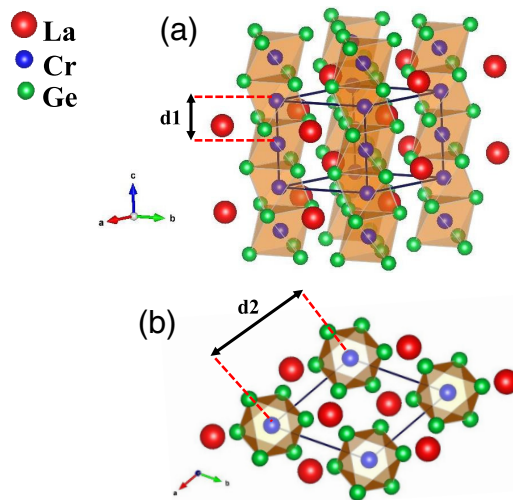


FIG. 5. Crystallographic structure of hexagonal perovskite-type ($P6_3/mmc$ space group) $RCrGe_3$ ($R = La, Ce$) viewed (a) perpendicular to the c direction in a polyhedral representation (b) in the ab plane. d_1 and d_2 are the intralayer and interlayer distances, respectively.

positions do not interfere with any magnetic peak positions, and thus have no influence on the magnetic refinements.

Figure 5 shows the crystallographic structure from the NPD pattern recorded in the paramagnetic state (at room temperature). The structure consists of octahedral chains formed by Ge face-sharing Cr centers separated by R atoms, and the Cr sublattice has a cubic structure. The R atoms occupy the $2d$ site ($1/3, 2/3, 3/4$), Cr atoms occupy the $2a$ site ($0, 0, 0$), and Ge atoms occupy the $6h$ site ($x, 2x, 1/4$) [2]. d_1 and d_2 are the intralayer (distance between two consecutive Cr atoms in the c axis) and interlayer (distance between two consecutive Cr atoms in the ab plane) distances, respectively. Results at room temperature are presented in Table II and the fit to the diffraction patterns are shown in Fig. 6.

NPD results for $LaCrGe_3$ measured at 5 K reveal a significant intensity enhancement for the (100) Bragg reflection when compared to that in the paramagnetic state at 110 K. This ferromagnetic peak at $2\theta = 22.5^\circ$ is the strongest mag-

netic peak (see Fig. 7). In addition, we have a small intensity enhancement for the (110) and (102) Bragg reflections. Finally, it is clear that there is a small shift in the positions of the (002) and (200) reflections due to the thermal variation of the lattice parameter and Debye-Waller factor and possibly a small magnetic contribution (see Fig. 8). All the magnetic intensities were found in the same position as the nuclear peaks, as expected for a ferromagnetic structure. The Cr spins are aligned along the c -axis direction, forming a pseudo-1D structure. Structural parameters for this sample are shown in Table III and present an ordered magnetic moment of $1.40(5) \mu_B$, which is due to the magnetic Cr atoms. This value is in good agreement with $1.31(4) \mu_B$ at 3 K for Cr spins aligned along the c axis from reference [12]. Lattice parameters for $LaCrGe_3$ [$a = 6.172(1) \text{ \AA}$ and $c = 5.742(1) \text{ \AA}$ at 120 K and $a = 6.166(1) \text{ \AA}$ and $c = 5.749(1) \text{ \AA}$ at 3 K] are in good agreement with those presented in previous studies [12].

NPD results for $Ce_{0.42}La_{0.58}CrGe_3$ and $Ce_{0.58}La_{0.43}CrGe_3$ measured at 5 K have revealed the same significant intensity enhancement for the (100) reflection when compared to the paramagnetic state at 100 K, as well as the small increase for (110) and (102) reflections (see Fig. 8). Consequently, we have analyzed these samples using the model with a single phase including structural and magnetic peaks with hexagonal $P6_3/mm'c'$ symmetry. The Cr spins are aligned along the c -axis direction. Figures 7 and 8 display the NPD and magnetic peaks, and Table III shows the structural and magnetic parameters obtained for all samples at 5 K.

In the case of $Ce_{0.81}La_{0.19}CrGe_3$ and $CeCrGe_3$, the NPD results at 5 K have shown not only a more evident (101) plane reflection than in the other samples when compared to that in the paramagnetic state measured at 100 K for $Ce_{0.81}La_{0.19}CrGe_3$ and 90 K for $CeCrGe_3$, but also an increase for the (100) and (102) reflections and possibly a very small contribution from the (002) and (200) reflections (see Fig. 8). It is clear from Fig. 8 that the intensity of the (100) reflection decreases whereas the intensity of the (101) reflection increases when the La concentration decreases. In this case, changes in the reflections could be related to a change in the magnetic moment value, change in the Cr spin orientation or, alternatively, a contribution from the Ce magnetic moment.

TABLE III. Structural and magnetic parameters obtained from the Rietveld refinement analysis of measurements taken at 5 K for the $Ce_{(1-x)}La_xCrGe_3$ ($x = 0, 0.19, 0.43, 0.58, 1$) series: Unit cell parameters (a and c), Ge atom position (x_{Ge} and y_{Ge}) and chi squared (quality of the fit) (χ^2). Cr ion magnetic moment (μ_{Cr}) along the c axis for $x = 0.19, 0.43, 0.58$, and 1, and for $CeCrGe_3$ in both directions along the c and parallel to the ab plane.

	$CeCrGe_3$	$Ce_{0.81}La_{0.19}CrGe_3$	$Ce_{0.58}La_{0.43}CrGe_3$	$Ce_{0.42}La_{0.58}CrGe_3$	$LaCrGe_3$
a (\AA)	6.112(1)	6.129(1)	6.140(1)	6.151(1)	6.169(1)
c (\AA)	5.696(1)	5.712(1)	5.723(1)	5.736(1)	5.752(1)
Occ(Ce)	—	0.82(2)	0.58(2)	0.42(1)	—
cc(La)	—	0.18(2)	0.43(2)	0.58(1)	—
x_{Ge}	0.1928(1) ^a 0.1927(1) ^b	0.1931(1)	0.1930(1)	0.1929(1)	0.1932(1)
y_{Ge}	0.3857(1) ^a 0.3855(1) ^b	0.3861(1)	0.3864(1)	0.3859(1)	0.3865(1)
μ_{Cr} (μ_B)	0.64(6) ^a 0.90(7) ^b	0.66(6)	0.77(6)	0.90(5)	1.40(5)
χ^2	1.524 ^a 1.559 ^b	3.79	1.282	1.904	2.937

^a μ_{Cr} along the c axis.

^b μ_{Cr} parallel to the ab plane.

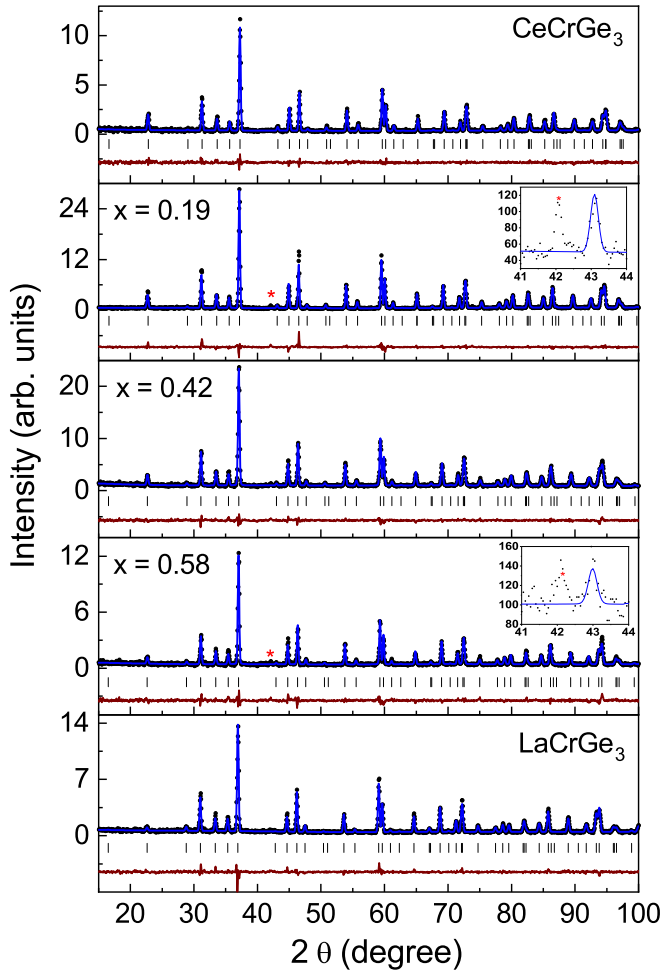


FIG. 6. NPD results with Rietveld refinement for $\text{Ce}_{(1-x)}\text{La}_x\text{CrGe}_3$ ($x = 0, 0.19, 0.43, 0.58, 1$) at room temperature. Blue continuous lines are the Rietveld refinement fit, red lines represent the difference between the observed and calculated intensities, and the small vertical black lines indicate the theoretical peaks position of the $P6_3/mmc$ space group. The peaks distinguished by the symbol * indicate the minor impurity phase ($\text{La}(\text{Ce})\text{Ge}_2$). Insets ($x = 0.19$ and $x = 0.58$) display the impurity peak. All error bars are shown and represent 1σ . However, the error bars may be smaller than the symbol.

Therefore, the refinement of NPD for CeCrGe_3 was analyzed with two models to describe the magnetic moments of the Cr ions. The first model is the same used for the other samples, considering the alignment of Cr spins parallel to c axis with $\mu_{\text{Cr}} = 0.636(63)\mu_B$. The second model comprises two phases, one with only structural peaks and the other with only magnetic peaks in the one-bar triclinic symmetry, resulting in the Cr spins aligned parallel to ab plane with $\mu_{\text{Cr}} = 0.903(75)\mu_B$. Figure 9 displays the Rietveld fit for each model. The magnetic moment of Ce atoms was not added to the model used to fit our NPD data because neither NPD results nor magnetization measurements, χ_{DC} and χ_{AC} revealed a coupling with the Ce ions. Thus, an ordered magnetic moment of Ce spins was not observed. We have tried to use the one-bar triclinic symmetry to refine NPD data from $\text{Ce}_{0.81}\text{La}_{0.19}\text{CrGe}_3$

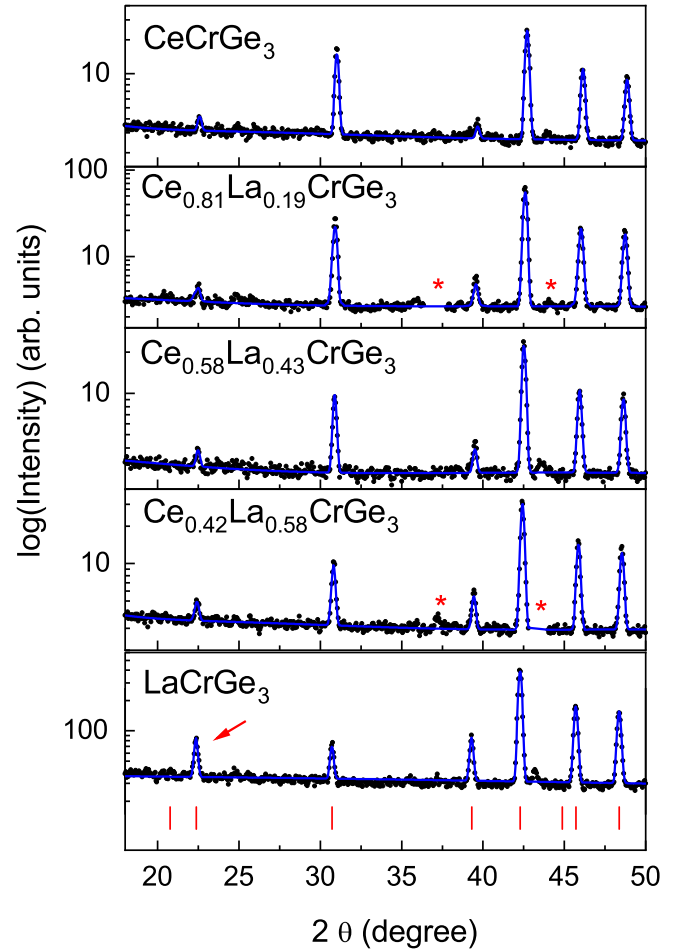


FIG. 7. NPD patterns of $\text{Ce}_{1-x}\text{La}_x\text{CrGe}_3$ ($x = 0, 0.19, 0.43, 0.58, 1$) at 5 K collected on BT1. Vertical red lines indicate the theoretical magnetic peak positions with hexagonal $P6_3/mmc$ symmetry (Cr spin align to the c axis). Arrow for the LaCrGe_3 pattern points to the FM peak at $2\theta = 22.5^\circ$. The peaks distinguished by the symbol * indicate the minor impurity phase [$\text{La}(\text{Ce})\text{Ge}_2$]. All error bars represent 1σ and are shown, but they may be smaller than the symbol.

sample but the model that fit better was the same one used for the LaCrGe_3 sample with Cr spins parallel to the c axis.

Results from both models are presented in Table III. The results of crystallographic parameters for CeCrGe_3 are in good agreement with those presented in previous studies [9] [$a = 6.1346(3)\text{ \AA}$ and $c = 5.7083(4)\text{ \AA}$ at 295 K]. The refinements with Cr spins oriented either along the c axis or parallel to the ab plane lead to quite different values of the structural and magnetic parameters. It was not possible to observe a significant difference between the two models used in the fits. Using the values in Table III for the Cr spins aligned along the c axis for CeCrGe_3 , it is clear that the values of the Cr magnetic moment, as well as the lattice parameters, gradually increase from $x = 0$ to $x = 1$, suggesting that this increase is caused by a chemical pressure as Ce ions are gradually substituted by La ions. The increase in the lattice parameters probably indicates that the Cr $3d$ band is less hybridized with a consequent increase in the magnetic moment. On the other

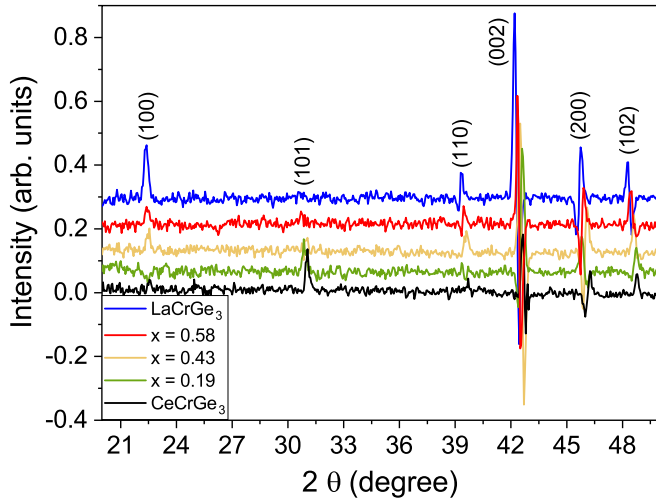


FIG. 8. Normalized magnetic intensity peaks from the difference in intensity between 5 K and high temperature in the paramagnetic phase for CeCrGe_3 , $\text{Ce}_{0.81}\text{La}_{0.19}\text{CrGe}_3$, $\text{Ce}_{0.58}\text{La}_{0.43}\text{CrGe}_3$, $\text{Ce}_{0.42}\text{La}_{0.58}\text{CrGe}_3$, and LaCrGe_3 . All error bars represent 1σ and are shown, but they may be smaller than the symbol.

hand, when the CeCrGe_3 magnetic moment is parallel to the ab plane, its value is higher than those for $x = 0.19$ and $x = 0.43$, suggesting an influence from Ce $4f$ spin which was not accounted for.

To show experimentally in which direction the Cr spins are aligned in this compound, we performed a NPD study for

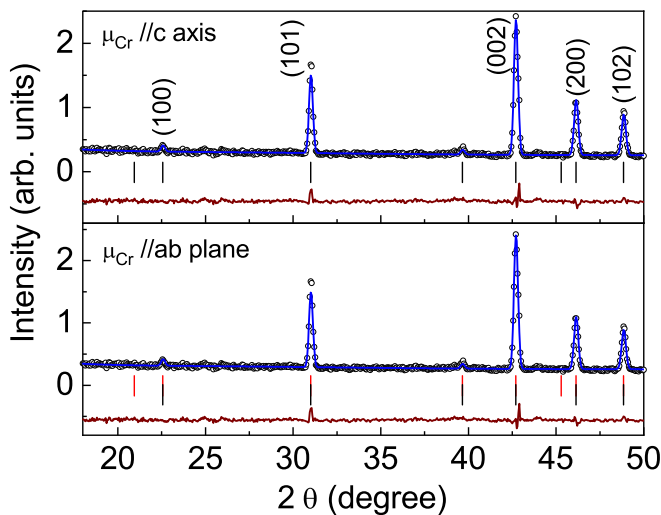


FIG. 9. NPD for CeCrGe_3 measured at 5 K with Rietveld refinement fit. Top: Direction of Cr magnetic moment (μ_{Cr}) along the c axis. Bottom: Direction of Cr magnetic moment parallel to the ab plane. Blue lines are the Rietveld refinement fit and brown lines are the residual. On the top, vertical black lines indicate the theoretical magnetic peak positions with hexagonal $P6_3/m\bar{m}'c'$ symmetry. On the bottom, vertical black lines indicate the position of theoretical peaks for the structural phase and vertical red lines indicate the theoretical magnetic peak positions with one-bar triclinic symmetry. All error bars represent 1σ and are shown, but they may be smaller than the symbol.

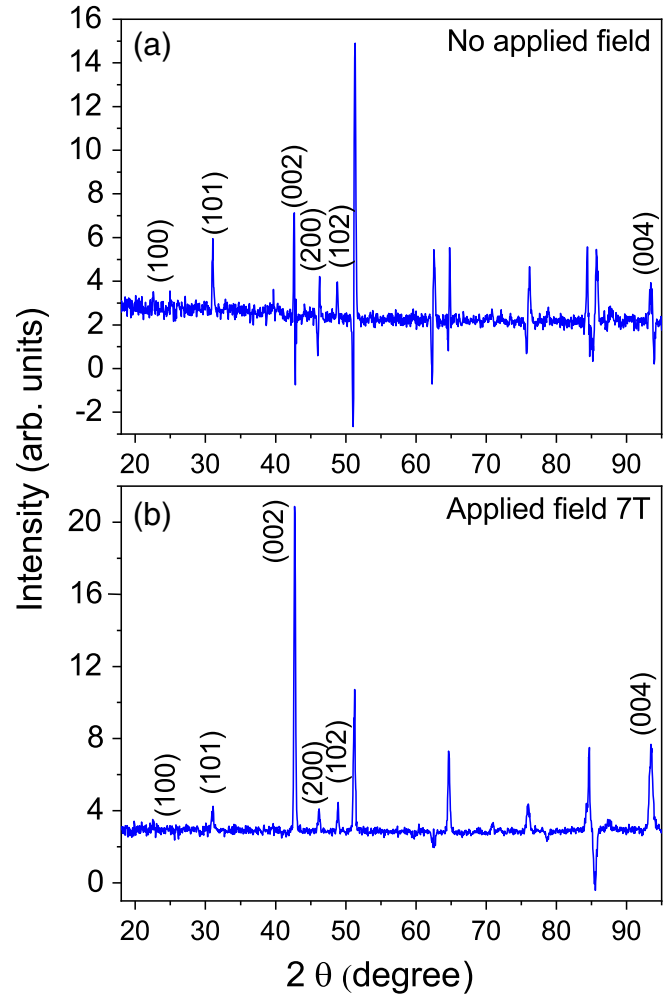


FIG. 10. CeCrGe_3 results. (a) Magnetic intensity peaks from the difference between 5 K and 90 K and (b) the difference between 0 T and 7 T at 5 K. All error bars represent 1σ and are shown but they may be smaller than the symbol.

CeCrGe_3 using a vertical field magnet system (7T VF) that applied an external magnetic field of 7 T. Figure 10 displays the pattern at 5 K with and without the application of the external magnetic field. From Fig. 10(b), one can observe the strong increase in the intensity of (002) and (004) plane reflections when compared to data from Fig. 10(a). This magnetic enhancement supports the idea that Cr spins in CeCrGe_3 are aligned parallel to the ab plane. Even with the application of an external field, no evidence of a Ce spin contribution can be observed from the NPD measurements. According to Das *et al.* [9], the magnetic contribution from the (101) reflection suggests ordering from Ce sublattice, but even with the application of a 7 T external field this reflection did not increase [see Figs. 10(a) and 10(b)].

The changes in the intensity for the (100) and (101) reflections when La ions are gradually replaced by Ce ions (see Fig. 8) is additional evidence that the Cr spins are aligned in different directions in these compounds, as previously commented.

TABLE IV. Magnetic Bragg peaks positions (2θ) for the (100) reflection and transition temperature ($T_C^{(BT-7)}$) obtained from neutron scattering at BT-7 triple-axis spectrometer for $Ce_{(1-x)}La_xCrGe_3$ ($x = 0, 0.19, 0.43, 0.58, 1$) series.

Sample	2θ (degrees)	$T_C^{(BT-7)}$ (K)
CeCrGe ₃	25.5	77(1)
Ce _{0.81} La _{0.19} CrGe ₃	25.7	82(1)
Ce _{0.58} La _{0.43} CrGe ₃	25.7	84(1)
Ce _{0.42} La _{0.58} CrGe ₃	25.8	92(1)
LaCrGe ₃	26	96(1)

2. Neutron scattering at BT-7 triple-axis spectrometer

To gain a better understanding about the magnetic transition, the BT-7 triple-axis spectrometer data were collected using the magnetic Bragg peak located at the (100) peak for all samples in the series. The position for the (100) plane in each sample is shown in Table IV. Figure 11 shows the measurements of the integrated magnetic Bragg peaks intensities, which presents a smooth increase as the temperature decreases below $T_C^{(BT-7)}$, indicating a second-order magnetic transition. This behavior is associated with the Cr site magnetic order. At low temperatures, the intensity exhibits the usual saturation that is typical of a conventional three-dimensional order parameter. Furthermore, the behavior for all samples show only one well-defined magnetic transition and it does not support the coexistence of both antiferromagnetic and ferromagnetic phases (as discussed in Appendix A). Specifically, for LaCrGe₃ the integrated intensity does not show any evidence of a spin reorientation, as suggested by χ_{DC} around 80 K. Thus, the divergence between the ZFC and FC curves, and the bump in the ZFC curve for LaCrGe₃ [see Figs. 1(a) and 2(a)], can be better explained by magnetic domains, in agreement with χ_{AC} data.

The fits of mean-field theory provide $T_C^{(BT-7)}$ for all samples and are displayed in Table IV. The results from CeCrGe₃ and LaCrGe₃ show a difference when compared to those previously reported [10]: $T_C = 73(1)$ K for CeCrGe₃ and $T_C = 88(1)$ K for LaCrGe₃.

IV. DISCUSSION

We have made a systematic investigation of the CeCrGe₃ structural and magnetic behavior, using magnetization measurements and neutron-scattering techniques as a function of doping La for Ce across the series to LaCrGe₃. The values of lattice parameters (a and c) and unit cell volume from NPD are displayed in Fig. 12. As expected, the gradual substitution of Ce by La leads to an increase in the lattice parameters and unit cell volume as a consequence of the well-known lanthanide expansion resulting in a bigger unit cell for LaCrGe₃, even though Ce ions have only one more 4f electron. As shown in Sec. III B, we have obtained a , c , and unit cell volume values for CeCrGe₃ and LaCrGe₃ at room temperature in good agreement with earlier published results.

Figure 13(a) shows the estimated $\mu_{eff}(y)$ and μ_{eff} obtained using the Curie-Weiss law for samples studied in this paper as a function of La concentration. From the estimated

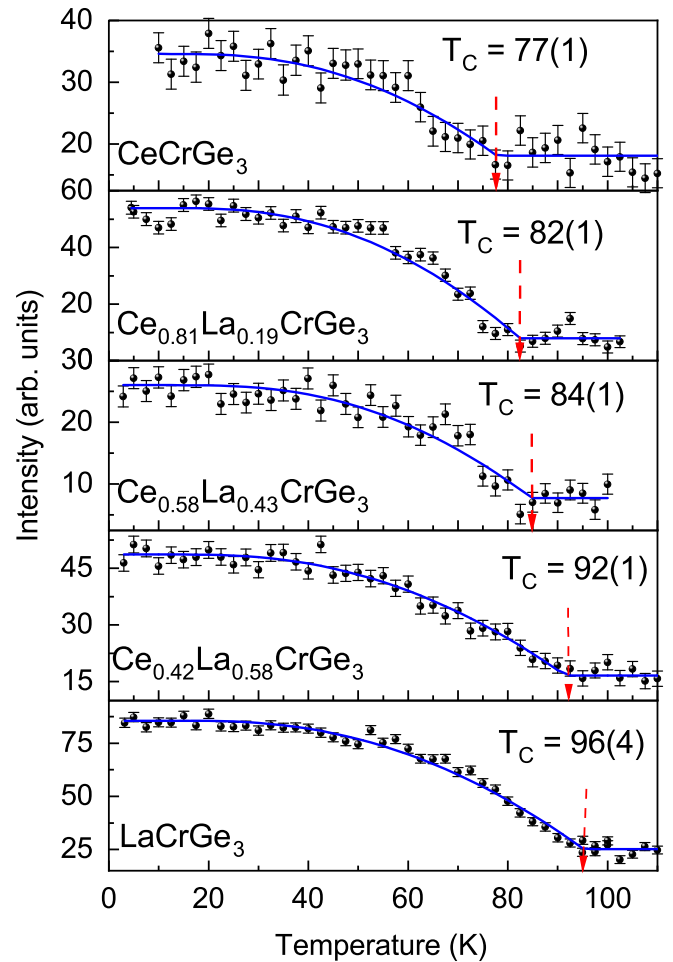


FIG. 11. Temperature dependence of the (1 0 0) integrated magnetic Bragg peak intensities. Because the (1 0 0) intensity is strong for LaCrGe₃ and weak for the Ce doped compositions, it was necessary to count longer to obtain sufficient signal to measure the order parameter. The blue solid curves show the mean-field function fit. The vertical red dashed arrows indicate the T_C obtained from the fit. All error bars are shown and represent 1σ . However, the error bars may be smaller than the symbol.

μ_{eff} , a linear behavior as a function of La concentration was expected. However, the results of Curie-Weiss analysis in the $Ce_{(1-x)}La_xCrGe_3$ ($x = 0, 0.19, 0.43, 0.58$) system show a nonlinear behavior, suggesting a higher contribution from the Ce^{3+} atoms for the $x = 0.43$ doped sample. Figure 13(b) plots the variation of $T_C^{(DC)}$, $T_C^{(AC)}$, and $T_C^{(BT-7)}$. The simplest explanation for this variation (for the same sample) is due to the different methods of calculating T_C not being identical. Beyond this, there are two possible origins for this variation: spin-glass behavior or domain-wall formation. In spin glasses, where the relaxation time of the spins is much longer than the period of the AC frequency, this variation is to be expected between $T_C^{(DC)}$ and $T_C^{(AC)}$. However, the AC susceptibility data do not show any variation with frequency and temperature. In contrast, domain-wall formation and then pinning, especially just below T_C , could result in a similar variation, as the different methods may be more or less sensitive to the degree of domain formation.

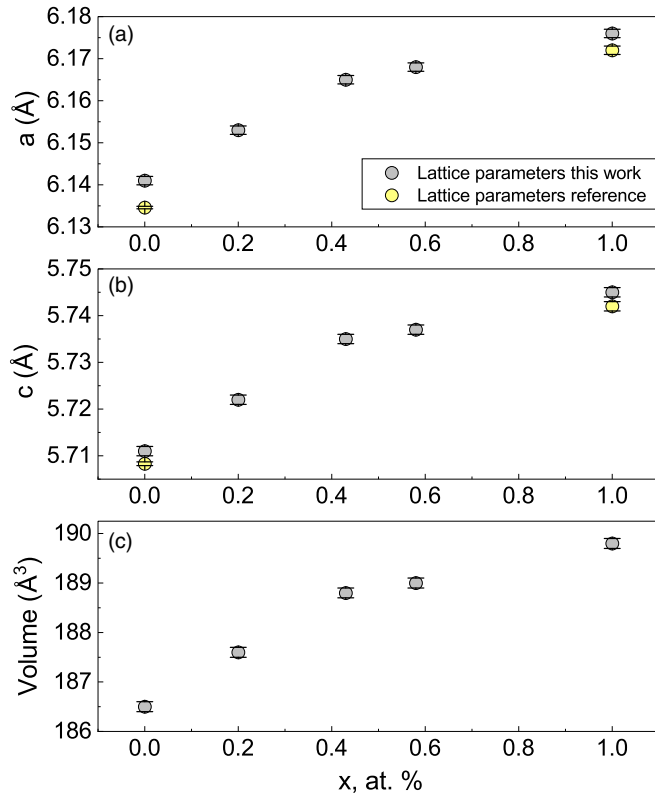


FIG. 12. Lattice parameters a , c , and unit cell volume at room temperature as a function of La doping at room temperature. The error bars represent 1σ .

In addition, T_C varies with the La concentration. It is known that the exchange interaction between the Cr atoms is based on the Cr-Cr distance along the c axis (interplanar) and in the a - b plane (intraplanar), both of which are mediated by Ge atoms. When the Ce in CeCrGe₃ is replaced with La, the unit cell volume increases and so do different transition temperatures. Knowing that the volume impacts T_C , a variety of factors, such as Ge vacancies, the presence of impurities, and disorder (Ge atoms occupying positions of Cr or La/Ce atoms), can contribute to the different transition temperatures. Therefore, the difference in T_C in the CeCrGe₃ and LaCrGe₃ when compared to those previously reported [2,8,10,12] can be influenced by the different methods used to synthesize the compounds.

Additionally, comparing Figs. 13(a) and 13(c), the values of μ_{Cr} are much lower than μ_{eff} . Such a difference suggests magnetic disorder reduces the spin polarization and consequently reduces the total ordered magnetic moment. In the case of Ce_(1-x)La_xCrGe₃ ($x = 0, 0.19, 0.43, 0.58$) this magnetic disorder could originate from the formation of domain walls at low temperature, where spin freezing may occur [15,16]. Considering that greater evidence of domain walls was seen in $x = 0$, $x = 0.19$, and $x = 0.43$ samples (see Sec. III A), that domain structure originates from magnetocrystalline anisotropy and is affected by defects in the crystal lattice [23] where the influence of Ce cannot be ruled out. For LaCrGe₃, as seen in the χ' and χ'' measurements,

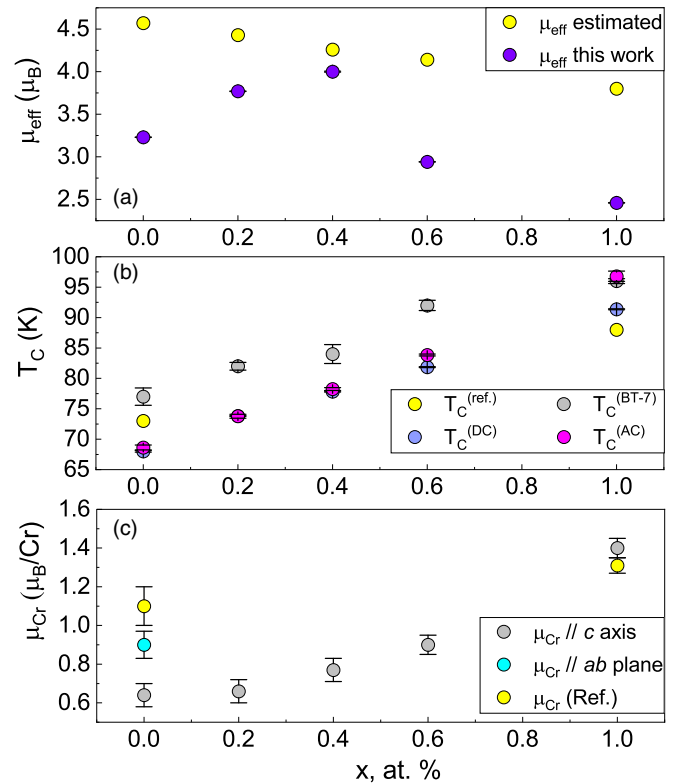


FIG. 13. (a) Effective magnetic moment (μ_{eff}), (b) transition temperature ($T_C^{(DC)}$, $T_C^{(AC)}$, and $T_C^{(BT-7)}$), and (c) magnetic moment of the Cr atoms (μ_{Cr}) from NPD as a function of La doping (x) at room temperature. The value μ_{Cr} in this paper is calculated in units of μ_B/Cr . [The value $\mu_{Cr}(Ref.)$ for CeCrGe₃ is parallel to the ab plane and for LaCrGe₃ is parallel to the c axis]. Error bars where indicated represent one standard deviation.

domain walls are also present and, similarly, at low temperatures, the spins freeze, causing this magnetic disorder [15,16].

The prime motivation of this paper was to determine the spin direction of Cr atoms in CeCrGe₃, because this information is not clear in literature. To address this question, NPD measurements with an external magnetic field of 7 T have been carried out. The results show an increase in the intensity of the magnetic peak corresponding to the (002) reflection, which shows that the moments align vertically along the field direction in the ab plane. Additionally, in contrast to the statement by Das *et al.* [9] on the coupling of Cr magnetic moments, the findings of the present paper do not reveal the coupling to the Ce spins, even under an external magnetic field at the temperature of 5 K. But, from $\chi_{AC}(T)$ results, there is a tendency of the Ce spins to order, suggesting an electron interaction of the Ce 4*f* bands with Cr *d* orbitals are energetically promoting Cr spins to align in parallel with the ab plane. We note that according to Nguyen, first-principles calculations show that LaCrGe₃ has a very strong peak just below the Fermi level, which is related to the Cr *d* orbital. The Cr spins delocalize with the application of external pressure [11]. Therefore, the replacement of La by Ce provides an external chemical pressure which causes a delocalization of Cr spins, changing their alignment direction. This is the simplest

explanation for the change in direction of the Cr spins from the c axis for LaCrGe₃ to the ab plane for CeCrGe₃.

V. CONCLUSIONS

In summary, we have investigated the structural and magnetic behavior of Ce_(1-x)La_xCrGe₃ ($x = 0, 0.19, 0.43, 0.58, 1$). The quality of samples was checked by XRD, magnetization measurements, and neutron diffraction techniques. CeCrGe₃, Ce_{0.58}La_{0.43}CrGe₃, and LaCrGe₃ have no detectable impurity phases whereas Ce_{0.81}La_{0.19}CrGe₃ and Ce_{0.42}La_{0.58}CrGe₃ present a small second phase of nonmagnetic La(Ce)Ge₂. Overall, results for CeCrGe₃ and LaCrGe₃ are consistent with other papers, and for $x = 0.19, x = 0.43$, and $x = 0.58$, results are in accordance with what is expected for doped compounds of this family. Curie temperatures from different techniques, $T_C^{(DC)}$, $T_C^{(AC)}$, and $T_C^{(BT-7)}$, differ, likely due to domain structure. The μ_{eff} agrees with the paramagnetic moment values as well as μ_{Cr} agrees with ferromagnetic moments values published previously for CeCrGe₃ and LaCrGe₃ compounds. The unit cell volume enhancement as a function of La-doping concentration is directly related to the increase

of T_C and magnetic moment. LaCrGe₃ and the doped compounds with $x = 0.19, x = 0.43$, and $x = 0.58$ present Cr spins aligned along the c axis direction, while CeCrGe₃ has the Cr spins aligned parallel to the ab plane. There is no evidence of Ce spin ordering.

ACKNOWLEDGMENTS

B.B.-S. thanks the financial support received from Coordenação de Aperfeiçoamento de Pessoal de Nível Superior (CAPES) by supporting postdoctoral research, Grant No. 88881.170115/2018-01. A.W.C. kindly acknowledges the Conselho Nacional de Desenvolvimento Científico e Tecnológico (CNPq) for support in the form of Grant No. 304627/2017-8. Partial financial support for this paper was provided by Fundação de Amparo a Pesquisa do Estado de São Paulo (FAPESP) under Grant No. 2014/14001-1. We thank Craig Brown for helpful discussions about the refinements. The identification of any commercial product or trade name does not imply endorsement or recommendation by the National Institute of Standards and Technology.

-
- [1] P. Manfrinetti, S. K. Dhar, R. Kulkarni, and A. V. Morozkin, *Solid State Commun.* **135**, 444 (2005)
- [2] H. Bie, O. Ya. Zelinska, A. V. Tkachuk, A. Mar, *Chem. Mater.* **135**, 4613 (2007)
- [3] H. Wang, J. Guo, E. D. Bauer, V. A. Sidorov, H. Zhao, J. Zhang, Y. Zhou, Z. Wang, Shu Cai, Ke Yang, A. Li, P. Sun, Yi-feng Yang, Qi Wu, T. Xiang, J. D. Thompson, and L. Sun, *Phys. Rev. B* **99**, 024504 (2019)
- [4] R. Khan, J. Yang, H. Wangand, Q. Mao, J. Du, B. Xu, Y. Zhou, Y. Zhang, B. Chen, and M. Fang, *Mater. Res. Express* **3**, 106101 (2016)
- [5] D. Das, A. Bhattacharyya, V. K. Anand, A. D. Hillier, J. W. Taylor, T. Gruner, C. Geibel, D. T. Adroja, and Z. Hossain, *J. Phys.: Condens. Matter* **27**, 016004 (2015)
- [6] X. Lin, V. Taufour, S. L. Bud'ko, and P. C. Canfield, *Phys. Rev. B* **88**, 094405 (2013)
- [7] V. Taufour, U. S. Kaluarachchi, S. L. Bud'ko, and P. C. Canfield, *Phys. B: Condens. Matter* **88**, 483 (2018)
- [8] V. Taufour, U. S. Kaluarachchi, R. Khasanov, M. C. Nguyen, Z. Guguchia, P. K. Biswas *et al.*, *Phys. Rev. Lett.* **117**, 037207 (2016)
- [9] D. Das, S. Nandi, I. da Silva, D. T. Adroja, Z. Hossain, *Phys. Rev. B* **94**, 174415 (2016)
- [10] D. Das, T. Gruner, H. Pfau, U. B. Paramanik, U. Burkhardt, C. Geibel, and Z. Hossain, *J. Phys.: Condens. Matter* **26**, 106001 (2014)
- [11] M. C. Nguyen, V. Taufour, S. L. Bud'ko, P. C. Canfield, V. P. Antropov, C.-Z. Wang, and K.-M. Ho, *Phys. Rev. B* **97**, 184401 (2018)
- [12] J. M. Cadogan, P. Lemoine, B. R. Slater, A. Mar, and M. Avdeev, *Solid State Phenom.* **194**, 71 (2013)
- [13] P. Lemoine, J. M. Cadogan, B. R. Slater, A. Mar, and M. Avdeev, *J. Magn. Magn. Mater. B* **325**, 135 (2013)
- [14] K. Binder and A. P. Young, *Rev. Mod. Phys.* **58**, 801 (1986)
- [15] J. D. Bocarsly, C. Heikes, C. M. Brown, S. D. Wilson, and R. Seshadri, *Phys. Rev. Mater.* **3**, 014402 (2019)
- [16] P. Nehla, Y. Kareri, G. D. Gupt, J. Hester, P. D. Babu, C. Ulrich, and R. S. Dhaka, *Phys. Rev. B* **100**, 144444 (2019)
- [17] V. N. Eremin, Z. K. Shi, Yu. I. Buyanov, and V. G. Batalin, *Powder Metall Met Ceram* **10**, 661 (1971)
- [18] A. Santoro, *J. Res. Natl. Inst. Stand. Technol.* **106**, 921 (2001)
- [19] A. C. Larson and R. B. Von Dreele, New Mexico, USA, Los Alamos National Laboratory Report LAUR. 6-784 (2000)
- [20] J. W. Lynn, Y. Chen, S. Chang, Y. Zhao, S. Chi, W. Ratcliff, II, B. G. Ueland, and R. W. Erwin, *J. Res. Natl. Inst. Stand. Technol.* **117**, 61 (2012)
- [21] R. T. Azuah, L. R. Kneller, Y. Qiu, P. L. W. Tregenna-Piggott, C. M. Brown, J. R. D. Copley, and R. M. Dimeo, *J. Res. Natl. Inst. Stand. Technol.* **114**, 341 (2009)
- [22] G. Amarotti and J. M. Fournier, *J. Magn. Magn. Mater.* **43**, L217 (1984)
- [23] E. M. Levin, V. K. Pecharsky, and K. A. Gschneidner, *J. Appl. Phys.* **90**, 6255 (2001).
- [24] B. Aslibeiki, P. Kameli, and H. Salamati, *Solid State Commun.* **149**, 1274 (2009).